NASA Technical Memorandum 86297

FAILURE ANALYSIS OF A GRAPHITE/EPOXY LAMINATE SUBJECTED TO BOLT BEARING LOADS

J. H. CREWS, JR. AND R. V. A. NAIK

AUGUST 1984

National Aeronautics and
Space Administration

Langley Research Center
Hampton, Virginia 23665

```
 8      1      1 RN/NASA-TM-86298
    SELECT     RN
    TERM IN SELECT COMMAND NOT IN DICTIONARY
================================================================================
 9      1      1 RN/NASA-TM-86297
          DISPLAY 09/2/1
     84N32436**    ISSUE 22    PAGE 3544    CATEGORY 24    RPT#: NASA-TM-86297 NAS
     1.15:86297    84/08/00  35 PAGES    UNCLASSIFIED DOCUMENT
UTTL: Failure analysis of a graphite/epoxy laminate subjected to bolt bearing
     loads
AUTH: A/CREWS, J. H., JR.;  B/NAIK, R. V. A.    PAA: B/(Old Dominion Univ.,
     Norfolk, Va.)
CORP: National Aeronautics and Space Administration. Langley Research Center,
     Hampton, Va.    AVAIL.NTIS    SAP: HC A03/MF A01
MAJS: /*FAILURE ANALYSIS/*GRAPHITE-EPOXY COMPOSITES/*LOADS (FORCES)/*TENSILE
     STRESS
MINS: / FINITE ELEMENT METHOD/ JOINTS (JUNCTIONS)/ MODES/ STRESS ANALYSIS/
     STRESS CONCENTRATION
ABA:  B.W.
ABS:  Quasi-isotropic graphite/epoxy laminates (T300/5208) were tested under
     bolt bearing loads to study failure modes, strengths, and failure energy.
     Specimens had a range of configurations to produce failures by the three
     nominal failure modes: tension, shearout, and bearing. Radiographs were
     made after damage onset and after ultimate load to examine the failure
     modes. Also, the laminate stresses near the bolt hole calculated for each
     test specimen configuration, and then used with a failure criterion to
     analyze the test data. Failures involving extensive bearing damage were
     found to dissipate significantly more energy than tension dominated
ENTER:
```

INTRODUCTION

Bolt loads can produce failures by one of three basic failure modes--tension, shearout, or bearing. However, joints are usually designed with little regard for failure modes and typically are optimized for maximum ultimate strength. For current graphite/epoxy composites, this approach usually leads to joints that fail in the tension mode. Unfortunately, such tension failures can develop with little advance warning in a rather catastrophic manner.

The objective of the present study was to analyze and compare laminate failures for each of the three basic failure modes. Toward this end, tests were conducted to measure damage onset strength, ultimate strength, and failure energy for specimens subjected to bolt-bearing loads. Specimens were 16-ply quasi-isotropic T300/5208 graphite/epoxy laminates in various configurations that were designed to produce the different failure modes. Radiographs, enhanced with a dye-penetrant, were used to observe the local damage. A finite-element stress analysis was conducted for each specimen configuration to determine how the configuration influenced the local stresses near the loaded hole. The computed stresses were also used with laminate failure criteria to predict failure modes and strengths.

Tests results are presented in terms of strength and failure energy plotted for the range of specimen configurations. Failure modes and sequences are identified and discussed. Stress results are presented as stress distributions and stress concentration factors. Failure predictions based on the stresses are discussed and compared with observed test results.

SYMBOLS

C	bolt-hole clearance, m
C_b	coefficient for bearing damage onset prediction
C_t	coefficient for tension damage onset prediction
d	hole diameter, m
e	specimen edge distance, m
K_{bb}	bearing stress concentration factor
K_{tb}	tension stress concentration factor
P	bolt load, N
r,θ	polar coordinates, m, deg
r_{ob}	characteristic dimension for bearing failure prediction, m
r_{ot}	characteristic dimension for tensile failure prediction, m
S_b	nominal bearing stress, MPa
S_{bo}	damage onset strength, MPa
S_{bu}	ultimate strength, MPa
t	laminate thickness, m
w	specimen width, m
x,y	Cartesian coordinates, m
δ	hole elongation, m
θ_c	bolt-hole contact half-angle, deg
σ	laminate stress, MPa
σ_{cu}	laminate compressive ultimate strength, MPa
σ_{rr}	radial stress component, MPa
σ_{tu}	laminate tensile ultimate strength, MPa
$\sigma_{\theta\theta}$	circumferential stress component, MPa

TEST PROCEDURES

Test specimen configuration and loading are shown in figure 1. All specimens were made from the same $(0/45/90/-45)_{2s}$ T300/5208 graphite/epoxy laminate which had a nominal thickness of 2.24 mm. Bolt holes were ultrasonically drilled with a diameter of 6.37 mm. The steel bolts had a nominal diameter of 6.35 mm, but their actual diameter was 6.32 mm. This produced a hole clearance C of 0.05 mm. The specimen width-to-hole diameter ratio, w/d, ranged from 2 to 8. The edge distance-to-hole-diameter ratio, e/d, ranged from 1.5 to 4.0. These specimen configurations were selected to produce failures by the three basic failure modes shown in figures 2(b), 2(c), and 2(d). The other failure modes in figure 2 will be discussed later.

The bolt-loading apparatus is shown in figure 3. A pair of steel clevis straps loaded the bolt in double shear; a friction grip reacted the load. The washers (12.7 mm diameter) between the clevis straps and the specimen (see fig. 3(c)) distributed the clampup torque load over an area around the bolt hole. All bolts were torqued to 5.65 N.m, a moderate clampup torque for a 6.35 mm bolt.

Inductive displacement transducers were used to measure bolt-hole elongation. The apparatus shown in figure 3(d) measured the relative displacement between the clevis and a small, stiff wire that rested against the edge of the hole under the bolt. To provide clearance for the wire, the bolt and the washers were slotted. The measured displacements were attributed entirely to hole elongation, since the clevis and bolt deflections were insignificant.

The curve of nominal bearing stress, S_b ($S_b = P/td$), versus hole elongation, δ, was recorded throughout each test. The tests were conducted using hole elongation as the servo control variable. The hole elongation was increased at a very slow rate (0.002 mm/s) until the ultimate strength was

reached. This procedure produced load-displacement records that were very sensitive to any localized damage near the bolt hole. This procedure also allowed the specimens to be unloaded after ultimate strength was reached. The unloading prevented the failure mode information (i.e., local damage) corresponding to ultimate strength from being masked by the gross damage caused by complete specimen failure. A typical recording of bearing stress against hole elongation (S_b versus δ) is shown in figure 4. The nonlinearity near the origin is due to clampup friction between the washers and the specimen. Results in reference 1 with a similar test apparatus showed that the friction force was only about 50 N for the clampup torque used in the present study. For higher load levels, the $S_b - \delta$ curves were essentially linear despite the nonlinear contact that developed between the hole and the clearance-fit bolt. This contact behavior will be discussed later in the stress analysis section.

The damage onset strength, S_{bo}, was determined using three independent methods. The start of nonlinearity in the $S_b - \delta$ curve was the first evidence of damage and was used to indicate damage onset, as shown in figure 4. At slightly higher loads, snapping and popping noises were heard. The first such audible noise was taken as the second indication of damage onset, and the corresponding point was marked on each $S_b - \delta$ record. As the loading progressed, abrupt drops or jumps would occur in the curve, also indicating sudden damage development. The first such drop was used for the third S_{bo} measurement. In some tests, specimens were unloaded immediately after the first audible noise was detected and then radiographed using an x-ray-opaque dye penetrant to determine the location, mode, and extent of damage. These specimens were not tested further. Most specimens were loaded to ultimate strength before they were unloaded and radiographed.

Specimens could not be unloaded precisely after ultimate load (point A) was reached; testing had to continue slightly beyond this point to be certain that it was the peak value for that curve. For example, the curve in figure 4 extends beyond point A to point B before unloading to point C. However, the unloading curve from point A was needed to calculate the failure energy. The failure energy was calculated from the area enclosed by the curve OAD. The desired unloading curve from point A was approximated, as shown in figure 4, by shifting the BC curve to get the AD curve.

ANALYTICAL PROCEDURES

Stress Analysis

Laminate stresses near the fastener hole were calculated using the NASTRAN finite-element program with isoparametric elements. The finite-element model shown in figure 5 corresponds to the largest test specimen ($w/d = 8$ with $e/d = 4$). Other specimen configurations were modeled by eliminating elements to change the w/d or e/d ratio as required. As a result, the mesh refinement near the hole was identical for all configurations. The mesh in this area consisted of small triangular elements, each subtending 0.9375°, as shown in figure 5. The distance to the grip line end of the model was 6d for all cases. A Young's modulus of 58.89 GPa and a Possion's ratio of 0.31 were used to represent the quasi-isotropic T300/5208 laminate. These properties were obtained using lamination theory and the T300/5208 ply properties from reference 2.

As previously mentioned, the case of a laminate with a clearance-fit, loaded hole is a nonlinear problem. The contact area between the bolt and the hole increases nonlinearly as a function of the bolt bearing stress, producing a changing boundary condition at the hole boundary. An analytial approach similar to that in reference 3 was used here to determine the nonlinear

relationship between the bearing stress, S_b, and the contact angle, θ_c. The bolt was assumed to be frictionless, rigid, and fixed and the grip-line end of the model was subjected to a uniform displacement, u_o, in the negative x-direction. Within a specified contact arc, θ_c, the nodes on the hole boundary were constrained to lie on a circular arc having the bolt radius. The bearing stress, σ_{rr}, at the end of the contact arc ($\theta = \theta_c$) should be zero when the proper combination of θ_c and u_o is found. The procedure started by assuming values of θ_c and u_o and then calculating σ_{rr} at $\theta = \theta_c$. A second u_o value was used with the same θ_c value and a second σ_{rr} was calculated at $\theta = \theta_c$. A linear extrapolation (or interpolation) was used to find the u_o value corresponding to $\sigma_{rr} = 0$. This u_o value along with the assumed θ_c value defined a point on a $u_o - \theta_c$ curve. The procedure was repeated to develop a $u_o - \theta_c$ curve for each specimen configuration. A similar procedure led to $S_b - \theta_c$ curves. After these nonlinear curves were established, the proper θ_c and u_o values could be found for any S_b value.

Failure Predictions

Damage initiation was assumed to be governed by the peak stresses at the hole boundary. Accordingly, tensile damage onset was predicted by setting the peak tensile stress at the hole equal to the ultimate tensile strength, σ_{tu}, for the laminate. Using the tensile stress concentration factor, K_{tb}, this produced the following equation:

$$C_t S_{bo} K_{tb} = \sigma_{tu} \qquad (1)$$

The C_t coefficient was introduced to account for the local stress gradient near the hole. Whereas the σ_{tu} value was obtained from coupons where a

relatively large volume of material was subjected to a uniform stress, the material near the hole is subjected to a stress gradient and the peak stress exists only over a small volume. As a result, the hole boundary strength exceeds σ_{tu}. The coefficient C_t attempts to account for this stress gradient effect and was computed by solving equation (1) for C_t using test data involving tensile damage. To predict tensile damage onset, equation (1) was rewritten using this C_t value.

$$S_{bo} = \sigma_{tu}/(C_t K_{tb}) \tag{2}$$

This empirical relationship is similar to that proposed in reference 4 to predict the ultimate strength of loaded holes.

A similar expression was found for bearing damage onset using the bearing stress concentration factor, K_{bb}, and the laminate compressive strength, σ_{cu}.

$$S_{bo} = \sigma_{cu}/(C_b K_{bb}) \tag{3}$$

For a given case, both equations (2) and (3) were used to predict S_{bo} values for the two different damage onset modes. The lower S_{bo} value was taken as the damage onset strength prediction and it also indicated the predicted failure mode.

Although the damage onset was predicted using hole boundary stresses, the ultimate strength S_{bu} was predicted using the well known Whitney-Nuismer point-stress approach (ref. 5). According to this approach, failure is predicted when the computed laminate stress (or stresses) satisfy a failure criterion at a characteristic distance from the hole boundary. The maximum stress failure criterion was used with the point-stress approach. For tensile failures, the characteristic dimension r_{ot} was found by fitting the strength

prediction procedure to a measured S_{bu} value corresponding to an observed tensile failure. This r_{ot} value was then used to predict failure for other cases by using the stress distributions computed for these cases. This procedure will be discussed further when the predictions are compared with test results.

RESULTS AND DISCUSSION

Test Results

Test results are presented for ranges of w/d values and then for e/d values. In each case, the damage onset strengths and failure modes are presented and discussed. Next, the ultimate strengths and failure modes are addressed. Finally, the measured failure energies are compared and discussed for the various failure modes. Throughout this section, data points typically represent the average of three or more test values.

Width effects. - Damage onset results are presented in figure 6 for w/d values ranging from 2 to 8 with $e/d = 4$. Data from the three damage onset detection techniques (nonlinearity onset, audible noise, and first drop) are compared in figure 6(a). For $w/d = 2$ and 3, the damage onset was in the local tension (LT) mode. ("Local" refers to damage that was confined to the region under the washer. Damage beyond this region will be referred to as "remote" damage.) Notice that for the small w/d values, nonlinearity was not observed. For larger w/d values, nonlinearity developed before audible noises and two modes of damage were detected, local bearing (LB) and local tension (LT). This suggests that LB damage caused the nonlinearity and LT damage caused the audible noise. The subsequent damage that caused the first drop in the $S_b - \delta$ curve could have been caused by larger scale, abrupt damage in either the LT or LB modes.

The damage onset locations are shown in figure 6(b). Except for $w/d = 2$, the LT damage occurred in the range of θ from 71° to 74°. The LT damage appeared to consist of lamina splitting and was concentrated in a small region extending transversely from the hole, as shown in figure 2(b). In contrast, the bearing damage appeared to be mostly delamination and was spread over a large arc centered about $\theta = 0°$ on the hole boundary. The curve labeled "$\sigma_{\theta\theta}$ peak" will be discussed later.

Ultimate strength results are compared with damage onset results in figure 7. Except for the $w/d = 2$ case, which failed abruptly in a net-section tension (NT) mode, the failure mode data for the ultimate strengths were found by unloading the specimens after the maximum test load was reached, as previously explained. Consequently, the failure modes associated with the post-ultimate response, culminating in complete specimen failure, may be different from those indicated in figure 7. Comparison of the failure modes for damage onset and for ultimate strength indicates failure sequences. For small w/d values, damage initiated in the LT mode and progressed in the tensile mode until specimen failure. As previously discussed, for $w/d > 3$, the damage apparently initiated in the LB mode, followed by LT damage which produced the audible noise. As the load was further increased, the damage progressed in both modes in a stable manner until the ultimate strength was reached. For $w/d > 5$, remote bearing (RB) failure mode was found after ultimate strength was reached and the specimen was unloaded, see figure 2(b). It is doubtful that this RB damage developed in a stable manner because it occurred beyond the clampup washer where the laminate had no lateral support. It probably developed abruptly at ultimate load. Notice that in figure 7, the transition from LT to RB failures occurred for $4 < w/d < 6$, the range commonly used in composite joints. Also for this important w/d

range, notice that damage initiates at stress levels that are as small as 61 percent of the ultimate strength.

Failure energy data are presented in figure 8. As expected, the tension-dominant failures (small w/d values) dissipated very little energy. Significantly higher energy levels were measured for the larger w/d cases. Part of this increase is due to the higher ultimate strengths for large w/d values. However, a significant part of the increase is believed to be attributable to the LB failure mode observed for the larger w/d cases. The lateral support provided by the bolt clampup allowed the local bearing deformation to progress in a somewhat stable manner. This stable LB damage progressed until the specimen reached its ultimate strength. Although damage also grew in the LT mode, this damage did not appear to dissipate much energy, as shown by the results for $w/d = 3$ in figures 7 and 8. If this is the correct interpretation of the dramatic increase in failure energy shown in figure 8 for the large w/d cases, it indicates that failure mode can have a strong influence on the toughness of composite joints. For some joint applications, the increase in failure energy for $4 < w/d < 6$ may be more important than the increase in strength in that w/d range.

Edge distance effects. - Damage onset results for $w/d = 8$ and a range of e/d values are presented in figure 9. Damage initiated either in the LT or LB modes. For the smallest e/d value, when the specimens were radiographed after an audible noise, only the LT mode was observed. This is further evidence that the audible noise was caused by LT damage. Notice that even for the smallest e/d value, the expected shearout mode was not observed. For large e/d values, nonlinearity developed before the first audible noise and both LB and LT damage was found when the specimens were unloaded. Consequently, as with the w/d data, these results suggest that

LB damage caused the nonlinearity onset and that LB damage preceded the LT damage. Figure 9(b) shows that LT damage developed near $\theta = 71°$ for the entire range of e/d values. The radiographs showed this damage in rather narrow radial bands extending from the hole, as shown in figure 2(f).

Figure 10 shows ultimate strength results for the e/d values tested. For the smallest e/d value, the specimens failed by the sequence of LT damage followed by remote shearout (RS) to the specimen edge, see figure 2(f). For the intermediate e/d values, the damage started with local bearing, followed by local tension, and ended with remote shearout, shown as LB/LT/RS in figure 10. For the larger e/d values, the failure sequences culminated in RB failures. Note that the $e/d = 4$ case in this figure corresponds to the $w/d = 8$ case shown previously in figure 7.

The failure energy results in figure 11 show the same trend as discussed earlier for the w/d cases. Although the radiographs showed that the RS mode resulted in considerable delamination, this mode apparently dissipated little energy. The larger failure energy measurements appear to correlate with the presence of bearing damage.

Local Stress Evaluation

Stresses computed around the hole boundary are plotted in figure 12 for three different cases. These stresses, the $\sigma_{\theta\theta}$ tangential stress and the σ_{rr} bearing stress, have been normalized by S_b for comparison. The dashed curves correspond to the stresses for an infinite laminate with a snug-fitting ($C = 0$) rigid bolt. This case provides good reference stress distributions because the contact angle does not change with applied bearing stress. Therefore, the contact angle ($\theta_c = 82°$) and the stress distributions shown as dashed curves apply for any level of bearing stress. The peak value of $\sigma_{\theta\theta}/S_b$ is 0.92, which agrees with the values of 0.91 and 0.92 from references 6

and 7, respectively. This agreement verifies the finite-element modeling used in the present study.

The dash-dot curves in figure 12 represent stress distributions for the largest test specimen ($w/d = 8$ with $e/d = 4$) with a snug-fitting ($C = 0$) bolt. The contact angle of 85° is only slightly higher than for the infinite laminate case but the $\sigma_{\theta\theta}/S_b$ peak value was 1.14, more than 20 percent larger than the reference case. This shows that even the largest specimen used in the present study only roughly approximated the infinite laminate behavior.

The solid curves in figure 12 show the stress distributions for the largest test specimen with a 0.05 mm clearance fit. In this case, as discussed earlier, the contact angle increases with applied bearing stress. The results shown correspond to $S_b = 664$ MPa (the measured damage onset stress for this test configuration); the contact angle was found to be about 70°. The solid curve has a peak $\sigma_{\theta\theta}/S_b$ value of 1.27. Comparison with the dash-dot curve shows that clearance fit increased the $\sigma_{\theta\theta}$ peak by more than 10 percent and shifted its location by 15°. This emphasizes the importance of modeling the clearance fit in the present stress analyses.

The peak values of $\sigma_{\theta\theta}/S_b$ and σ_{rr}/S_b, expressed as stress concentration factors K_{tb} and K_{bb}, respectively, were calculated for the w/d and e/d ranges used in the test program. The applied bearing stress levels used in these calculations correspond to the damage onset strengths presented earlier in figures 7 and 10. The computed K_{tb} and K_{bb} results are plotted in figure 13. As expected, the small w/d cases had high K_{tb} values. The locations of $\sigma_{\theta\theta}$ peaks on the hole boundary are shown in figure 6(b). These locations agree well with the observed locations for tensile damage onset as

shown in figure 6(b). In contrast to the K_{tb} results, the K_{bb} values in figure 13(a) are virtually unaffected by the w/d ratio.

The K_{tb} values in figure 13(b) are elevated for smaller e/d ratios. This trend is probably responsible for the local tension damage previously observed for the test cases with small e/d values. This will be further discussed when strength predictions are presented in the next section. The locations for the $\sigma_{\theta\theta}$ peaks, corresponding to the K_{tb} results, are shown in figure 9(b). Again the locations for $\sigma_{\theta\theta}$ peaks agree very closely with the measured locations for tension damage onset.

Failure Predictions

The dashed curves in figure 14 are predictions for damage onset, obtained by using the calculated K_{tb} and K_{bb} values in equations (2) and (3). The laminate strengths used in these predictions were 414 MPa and 455 MPa for the tension and compression, respectively (ref. 2). The value of the C_t coefficient was determined from equation (1) using the S_{bo} data for the w/d = 2 case, which involved only tension damage. Tension damage predictions agreed reasonably well with the test data shown by open symbols. For the bearing predictions, C_b was found using S_{bo} data for the w/d = 4 case. For the small w/d ratios, the tension-damage curve lies below the bearing curve, indicating tension as the predicted damage onset mode. For w/d values greater than 4, bearing is the predicted mode. These trends agree with the observed failure modes discussed earlier.

The dot-dash curves in figure 14 are predictions for ultimate strength. The point-stress procedure was used with the σ_{xx} stress distributions and the maximum-stress failure criterion to calculate these curves. The σ_{xx} distributions used in this procedure were those calculated along the observed direction of damage growth. For tension predictions, the growth directions

were transverse lines that intersected the hole boundary at the observed damage onset locations, shown earlier in figure 6(b). The characteristic dimension r_{ot} for tension was found to be 1.54 mm, based on the $w/d = 4$ data, and that value was used to predict tension failure strengths for the other w/d values. The procedure was applied in a similar manner to obtain the predicted curve for bearing failure strengths. The bearing predictions were all based on σ_{xx} distributions along the x-axis. The characteristic bearing dimension r_{ob} was found to be 2.79 mm based on data from the $w/d = 6$ case. Comparison of the two dash-dot curves shows that bearing damage is predicted for $w/d \geq 6$, which agrees with the failure mode data shown in figure 7. Furthermore, the strength predictions agree reasonably well with the test results (solid symbols) in figure 14.

Figure 15 shows strength predictions for the e/d values. The damage onset predictions (dashed curves) were calculated using C_t and C_b values determined from the w/d results. For this reason these curves are not as accurate as for w/d predictions. Nevertheless, these curves predict the damage onset modes correctly and also predict the proper damage sequence for the large e/d cases. Because local shearout (see fig. 2(b)) was a viable failure mode for small e/d values, the shear stresses along the shearout plane ($y = d/2$) were determined for applied bearing stresses equal to the measured S_{bo} values. Even for the rather extreme case of $e/d = 1.5$, the maximum shear stress on this plane was slightly below the laminate shear strength (310 MPa, ref. 2). In contrast, the corresponding σ_{xx} stresses along the observed damage path (a radial line at $\theta = 71°$) exceeded the tensile ultimate strength by as much as 70 percent. This explains why the damage initiated in tension and propagated along the $\theta = 71°$ radial line rather than in the shear mode along the local shearout plane.

The predicted curve for remote shearout failures was calculated using the σ_{xx} distribution along the $\theta = 71°$ direction. As previously discussed, the failure sequence for the smaller e/d cases started as a tension failure along the $\theta = 71°$ path followed by remote shearout failure along the $y = d$ plane, see figure 2(f). The predicted dash-dot curve in figure 15 indicates the data trends but the predicted strengths have errors as large as 20 percent. Comparison of the two predicted dash-dot curves indicates the proper failure mode trends but not with as much accuracy as shown for the w/d cases.

The strength prediction procedures were also used with several failure criteria in addition to the maximum stress criterion. These other criteria were the Tsai-Hill (ref. 8), Tsai-Wu (ref. 9), Hoffman (ref. 10), Yamada-Sun (ref. 11), and the maximum strain criteria. The results based on the maximum strain criteria were almost as good as those based on maximum stress. However, none of the other criteria produced satisfactory predictions. Note that all of these other criteria involve multi-axial stress components. This suggests that the failures were governed primarily by the maximum stress, which in all cases was the x-axis stress component.

CONCLUDING REMARKS

Quasi-isotropic graphite/epoxy laminates (T300/5208) were tested under bolt-bearing loads using a simple fixture with a 6.35 mm steel bolt. Test specimens had a range of widths and edge distances to produce failures by several different modes. Radiographs were made after damage onset and after ultimate load to examine the failure modes and the failure sequences. The laminate stresses near the bolt hole were calculated for each test specimen configuration using a finite-element procedure. These stresses were then used in a failure prediction procedure to analyze the test results.

Damage onset was found to develop at stress levels that were as low as 62 percent of specimen ultimate strength. This damage developed in either the bearing mode or the tension mode. Even specimens with small edge distances developed damage in the tension mode rather than the shearout mode. Except for specimens with very small widths or edge distances, the first damage usually developed in the bearing mode and consisted mainly of ply delamination. However, at slightly higher stress levels, tension damage appeared in the form of ply cracks. The location of tension damage on the hole boundary correlated very well with the location of the computed maximum tensile stress. The stress analysis showed that both the location and magnitude of this maximum stress are strongly influenced by the bolt clearance.

The failure modes associated with ultimate strength were usually different from the damage onset mode. Only for the case of tensile failures in narrow specimens did the damage initiate and grow to failure in the same mode. When wide specimens were tested to ultimate strength, they first developed damage in the local bearing mode at the hole boundary, then local tensile damage (also at the hole boundary), and finally developed remote bearing immediately beyond the clampup washer. Specimens with moderately small edge distances also failed in a sequence involving three modes: damage appeared first in the local bearing mode, then in the local tension mode which lead to the remote shearout mode extending from the edge of the washer.

Failures involving extensive bearing damage were found to dissipate significantly more energy than tension dominated failures. Because the specimen configuration influenced the failure mode it, therefore, also influenced the failure energy. With increasing w/d values, for example, the transition from tension failure to bearing failure that occurred in the range of $4 < w/d < 6$ caused a very large increase in failure energy. For some

applications, this increase in failure energy for $4 < w/d < 6$ may be more important than the increase in strength in that range. The failure energy for bearing-loaded holes is a material property that should be given additional emphasis in joint design procedures as well as in material development activities.

REFERENCES

1. Crews, J. H., Jr.: Bolt-Bearing Fatigue of Graphite/Epoxy Laminate. Joining of Composite Materials, ASTM STP 749, K. T. Kedward, Ed., American Society for Testing and Materials, 1981, pp. 131-144.

2. DOD/NASA Advanced Composites Design Guide, Vol. IV-A: Materials, First Edition, Contract No. F33615-78-C-3203, Air Force Wright Aeronautical Laboratories, July 1983. (Available as NASA CR-173407 and from DTIC as AD B080 184L.)

3. Mangalgiri, P. D.; Dattaguru, B.; and Rao, A. K.: Finite Element Analysis of Moving Contact in Mechanically Fastened Joints. Proceedings of the Seventh International Seminar on Computational Aspects of the Finite-Element Method (CAFEM-7), Chicago, Illinois, Aug. 29-30, 1983, pp. 123-157.

4. Hart-Smith, L. J.: Bolted Joints in Graphite-Epoxy Composites. NASA CR-144899, National Aeronautics and Space Administration, Jan. 1977.

5. Whitney, J. M.; and Nuismer, R. J.: Stress Fracture Criterion for Laminated Composites Containing Stress Concentrations. J. Composite Materials, Vol. 8, July 1974, pp. 253-265.

6. DeJong, Theo: Stresses Around Pin-Loaded Holes in Elastically Orthotropic or Isotropic Plates. J. Composite Materials, Vol. 11, July 1977, pp. 313-331.

7. Eshwar, V. A.; Dattaguru, B.; and Rao, A. K.: Partial Contact and Friction in Pin Joints. Rep. No. ARDB-STR-5010, Dep. Aeronaut. Eng., Indian Inst. Sci., Dec. 1977.

8. Tsai, S. W.: Strength Theories of Filamentary Structures, Fundamental Aspects of Fiber Reinforced Plastic Composites, R. T. Schwartz and H. S. Schwartz, editors, Wiley Interscience, New York, 1968, pp. 3-11.

9. Tsai, S. W.; and Wu, E. M.: A General Theory of Strength for Anisotropic Materials. J. Composite Materials, Vol. 5, Jan. 1971, pp. 58-80.

10. Hoffman, O.: The Brittle Strength of Orthotropic Materials. J. Composite Materials, Vol. 1, 1967, pp. 200-206.

11. Yamada, S. E.; and Sun, C. T.: Analysis of Laminate Strength and Its Distribution. J. Composite Materials, Vol. 12, July 1978, pp. 275-284.

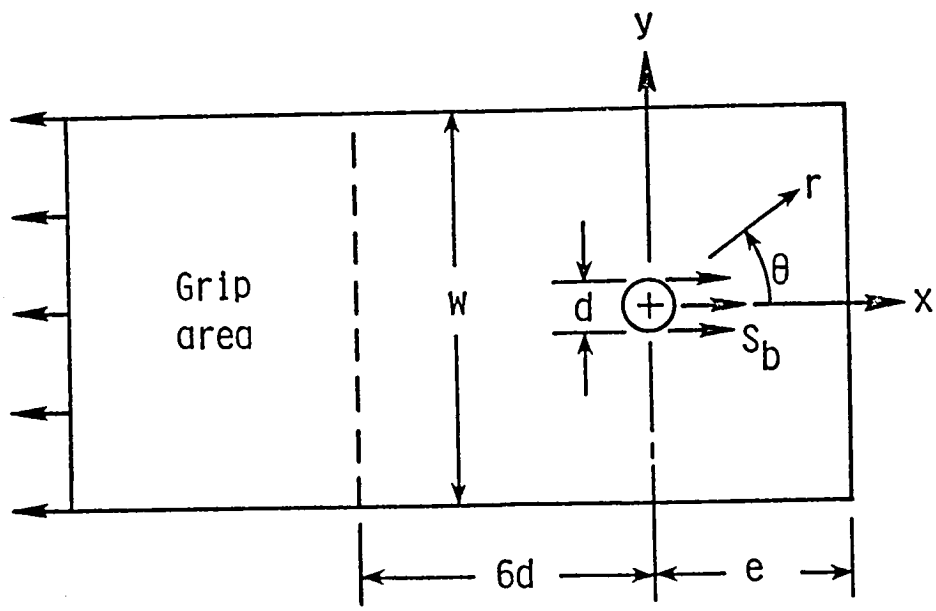

(a) Specimen configuration and loading

w/d	2	3	4	6	8	8	8	8	8
e/d	4	4	4	4	4	3	2.5	2	1.5

(b) Test specimen configurations

Figure 1. - Test specimen configurations and loading.

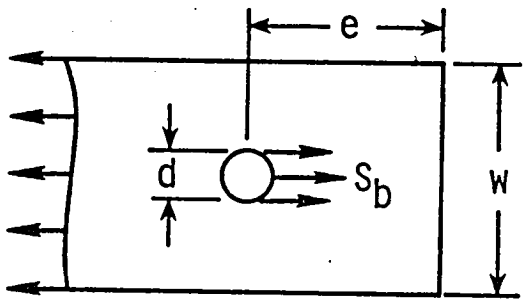

(a) Specimen configuration.

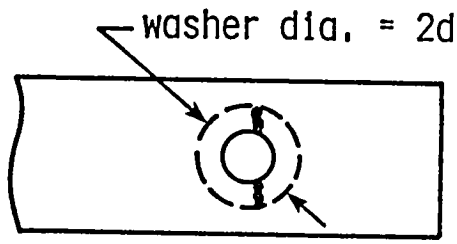

(b) Local tensile (LT).

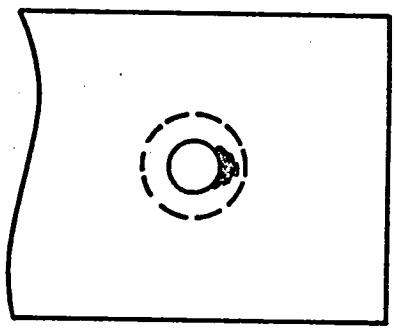

(c) Local bearing (LB).

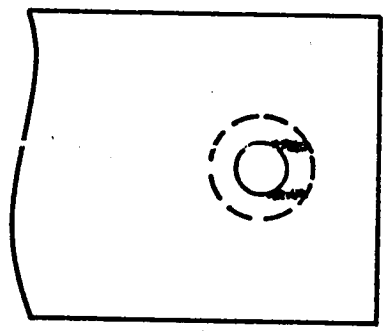

(d) Local shearout (LS)

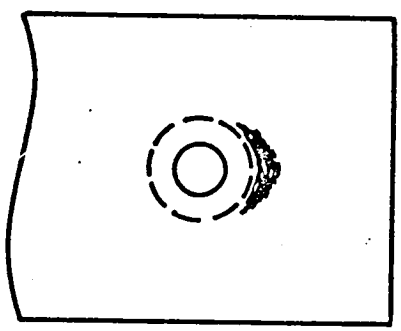

(e) Remote bearing (RB).

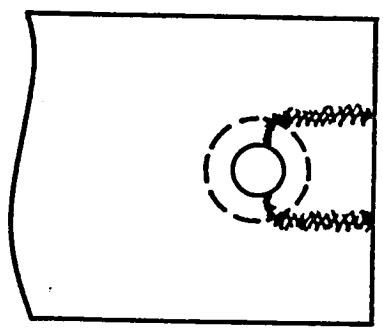

(f) Local tensile and remote shearout (LT/RS).

Figure 2. - Failure modes for loaded holes.

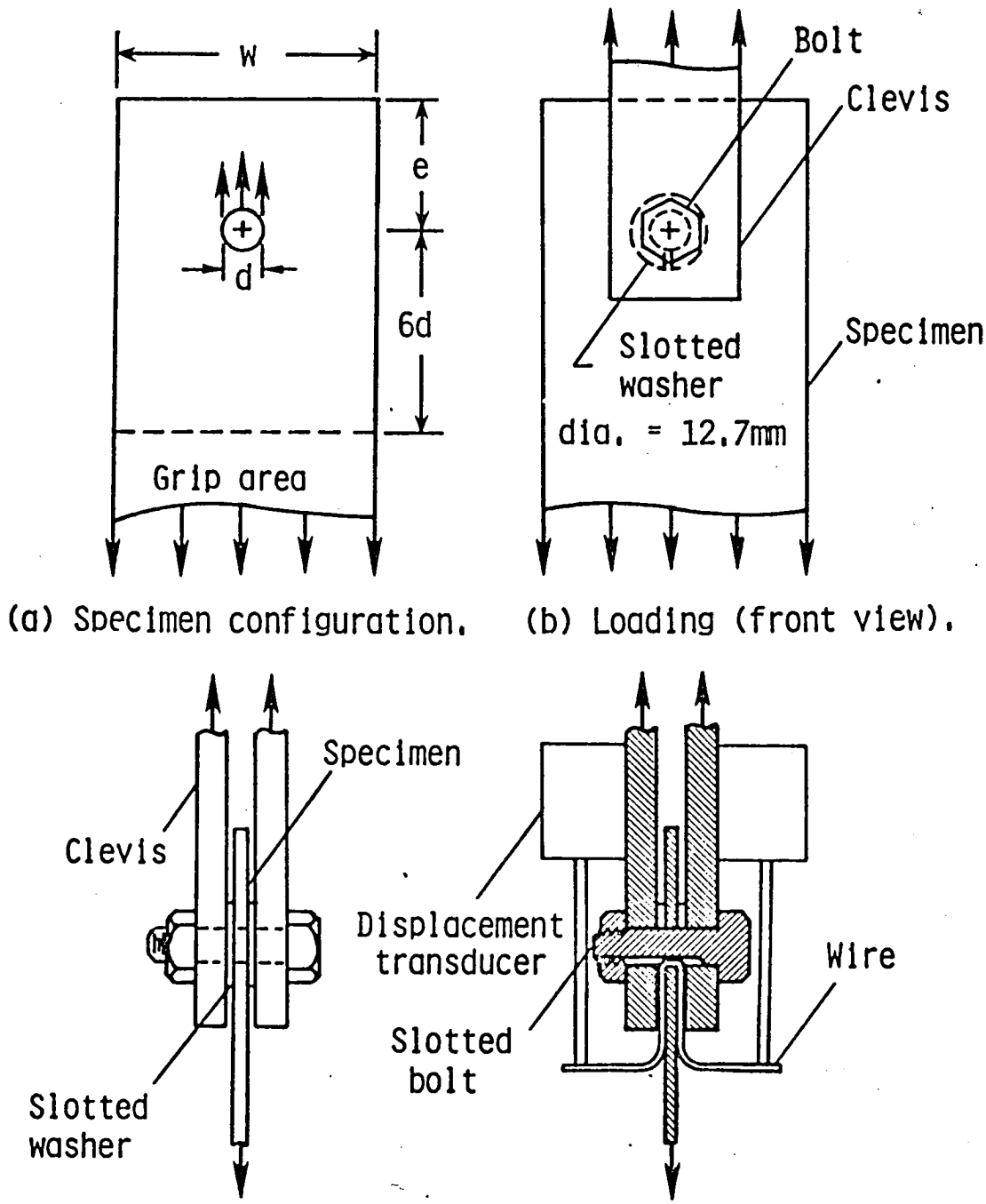

(a) Specimen configuration. (b) Loading (front view).

(c) Loading (side view). (d) Instrumentation.

Figure 3. - Specimen and test apparatus.

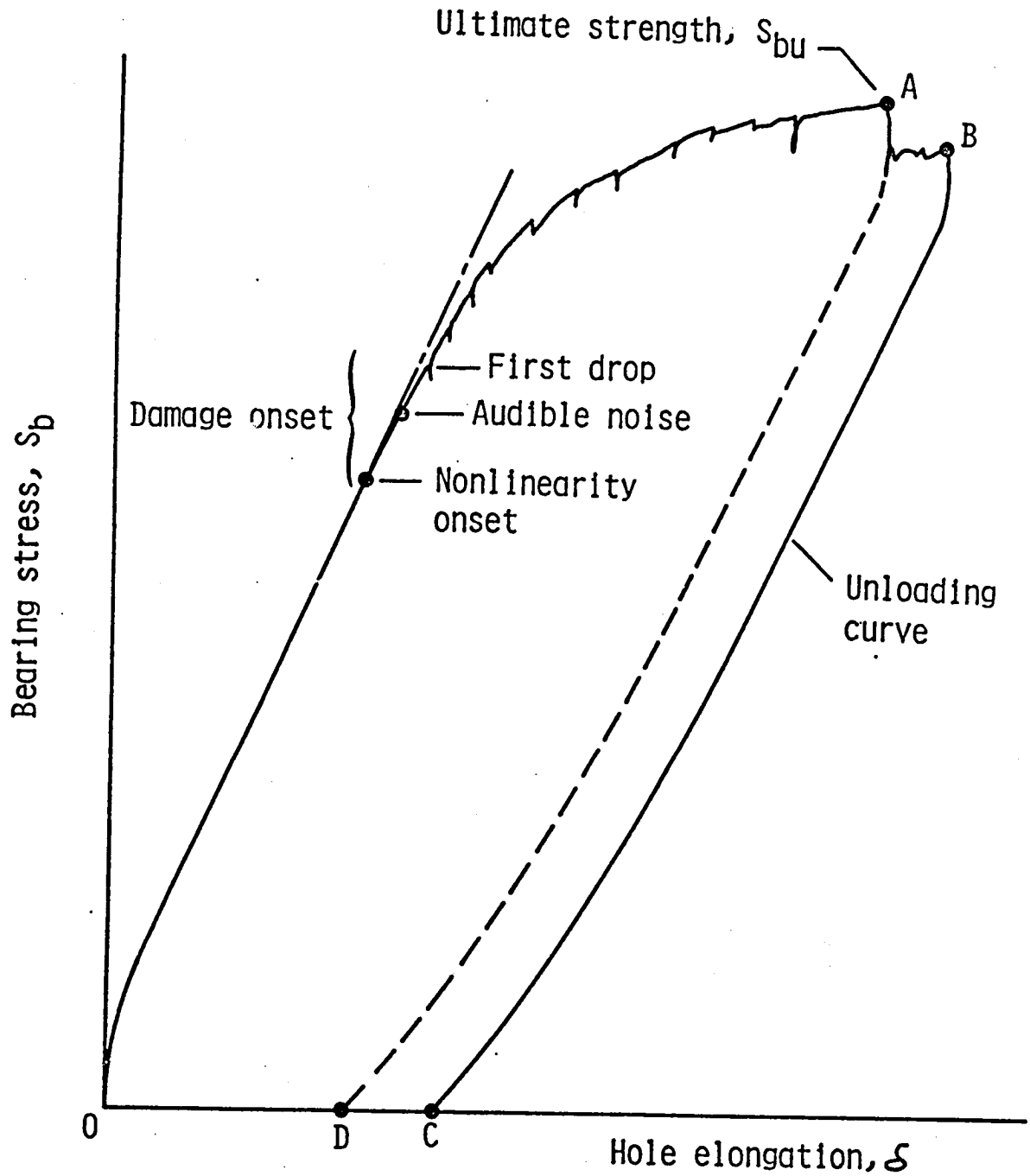

Figure 4. - Typical recording of bearing stress against hole elongation.

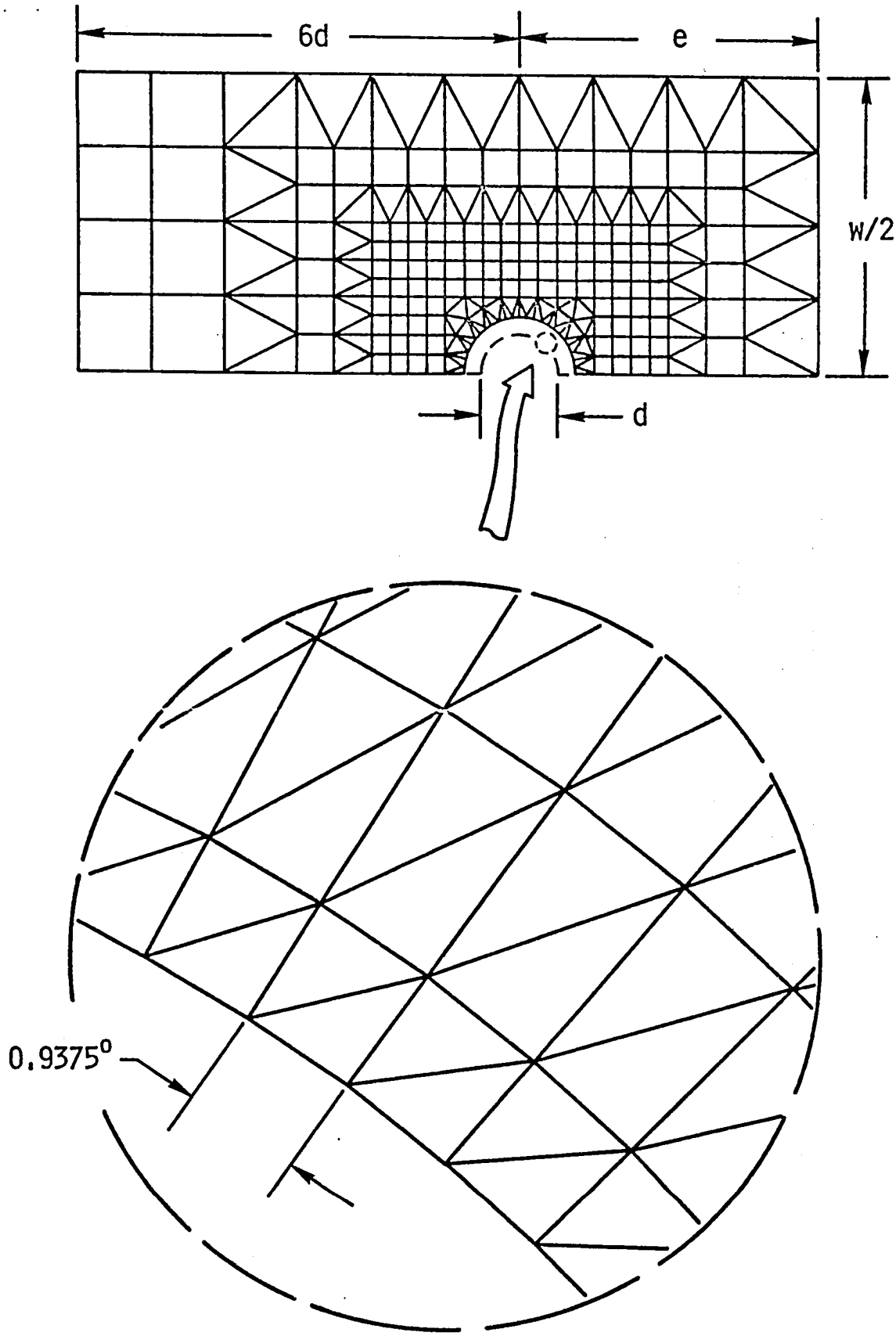

Figure 5. - Finite element model.

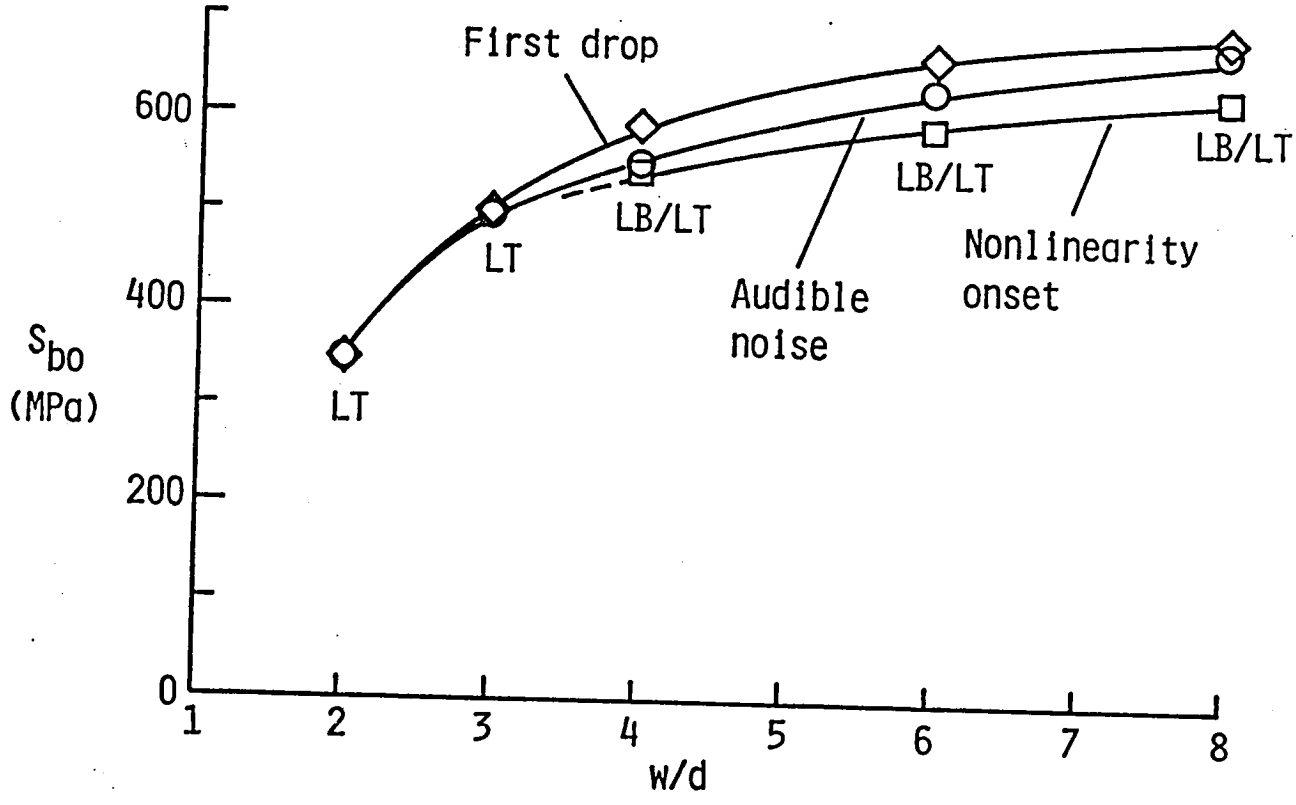

(a) Measured damage onset strengths.

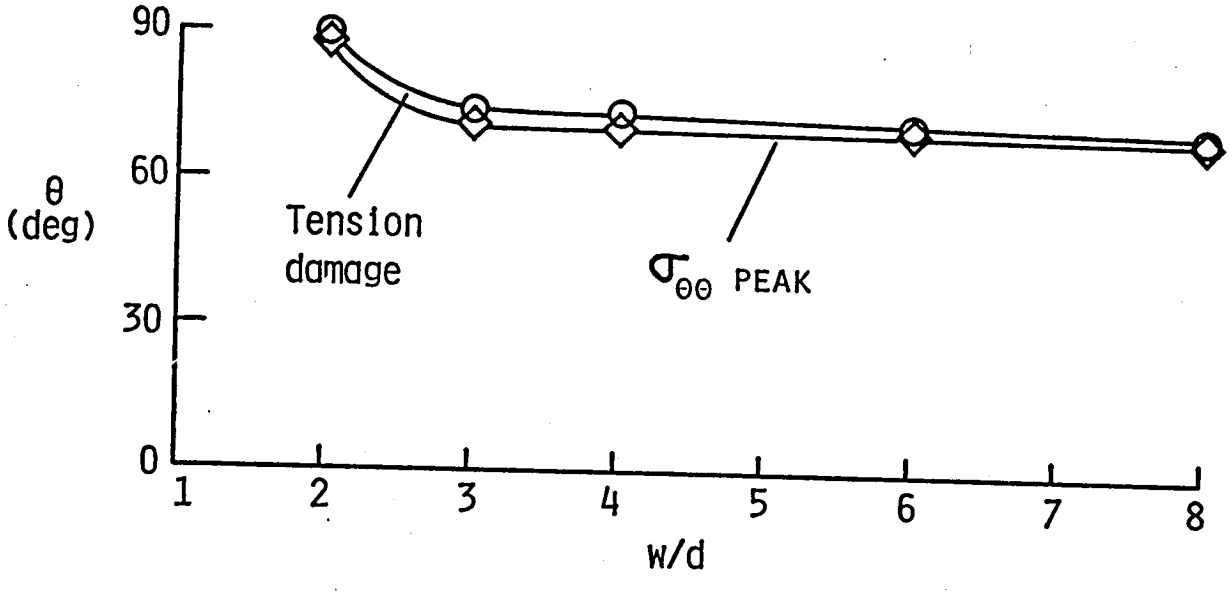

(b) Damage location on hole boundary.

Figure 6. - Damage onset results for W/d range, e/d = 4.

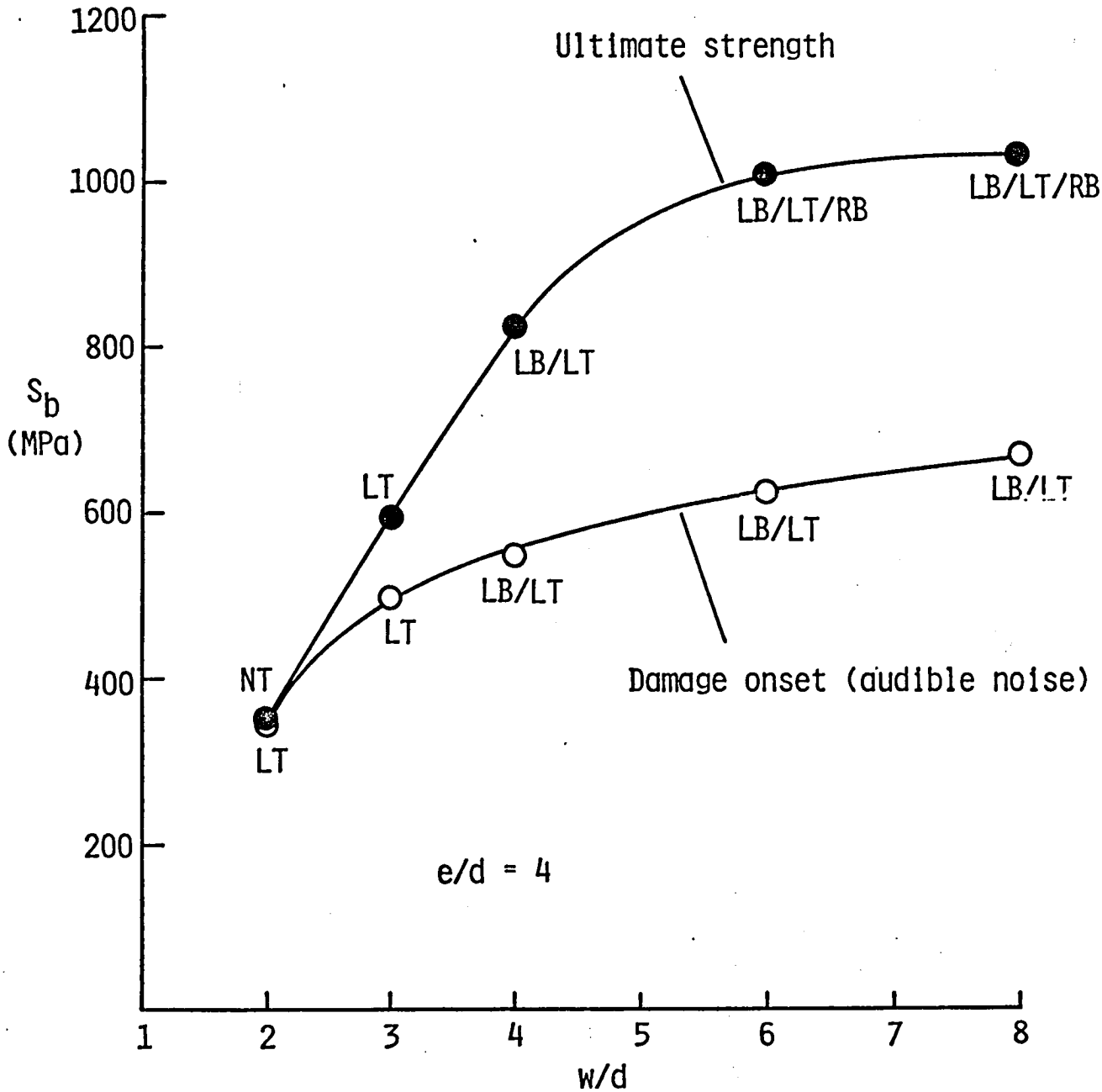

Figure 7. - Damage onset and ultimate strength for a range of w/d values.

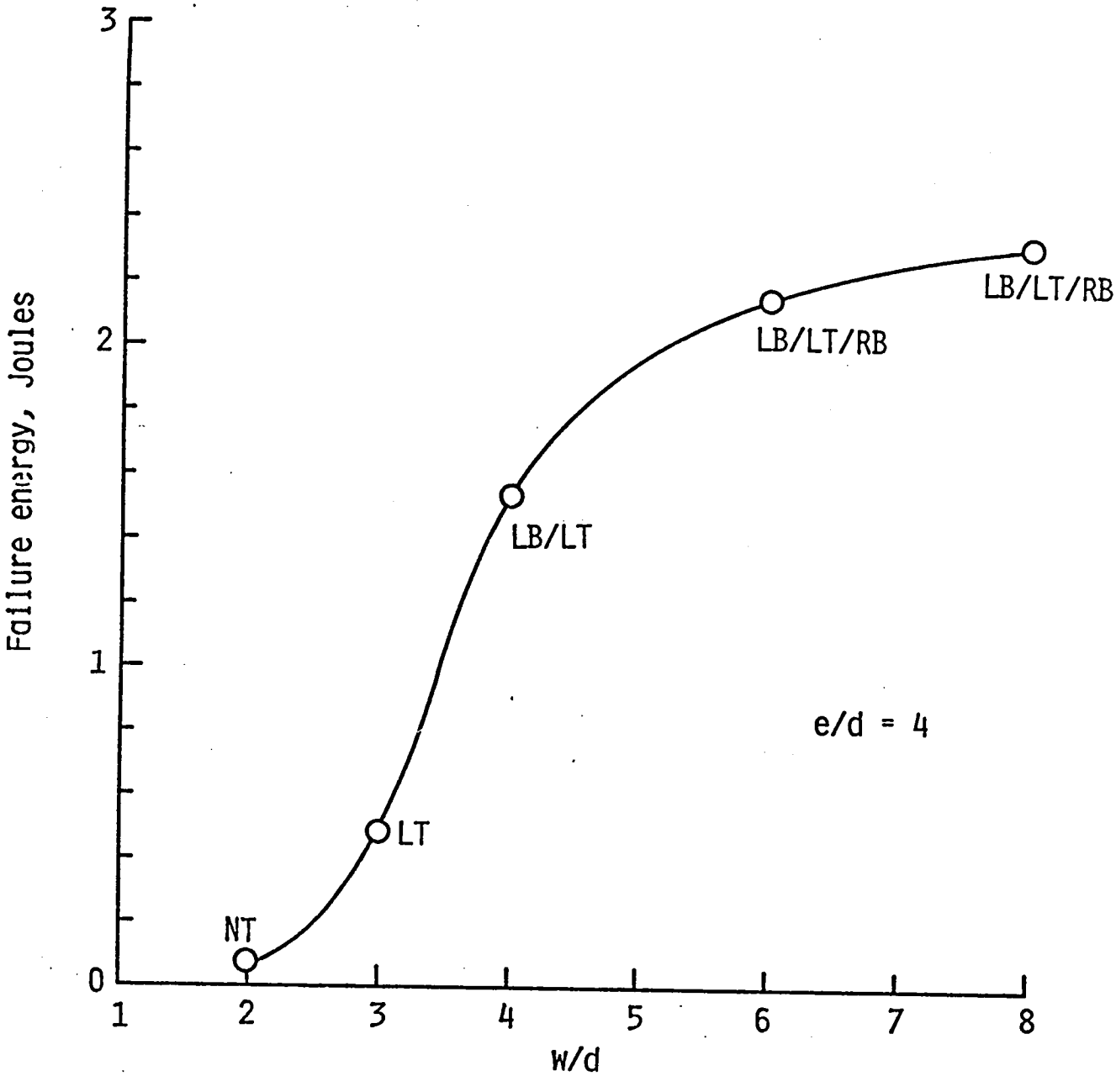

Figure 8. - Failure energy for range of w/d values.

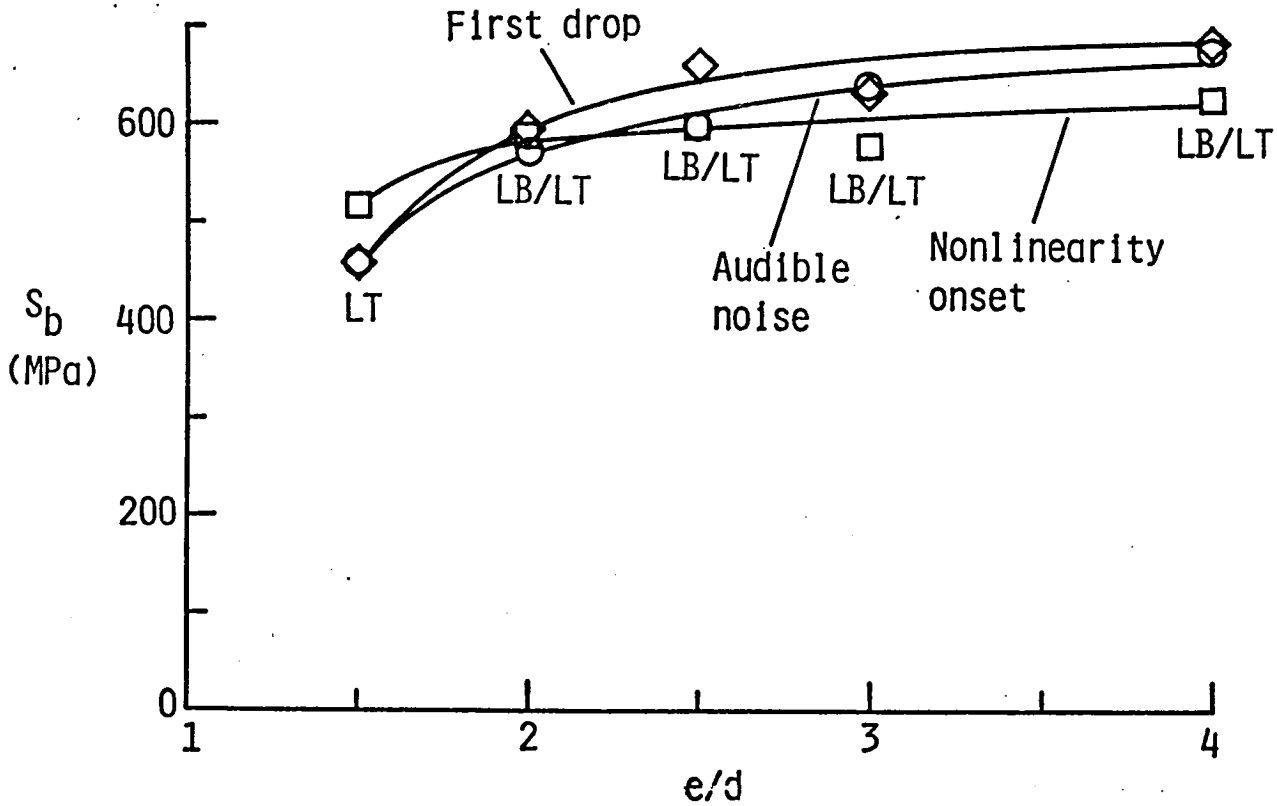

(a) Measured damage onset strengths.

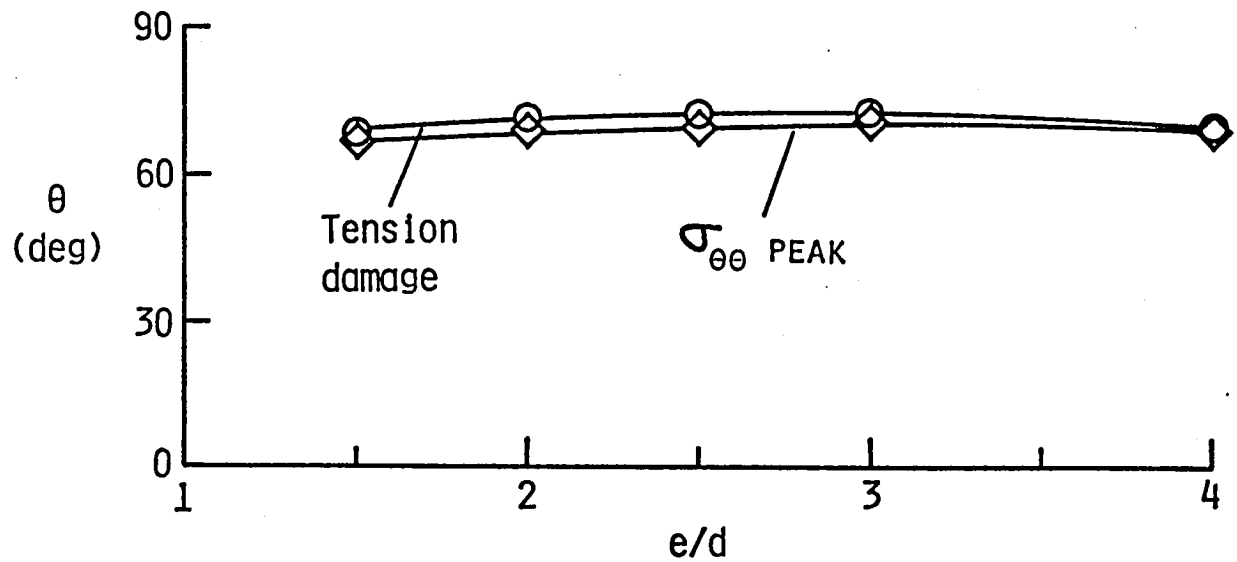

(b) Damage location on hole boundary.

Figure 9. - Damage onset results for e/d range, w/d = 8.

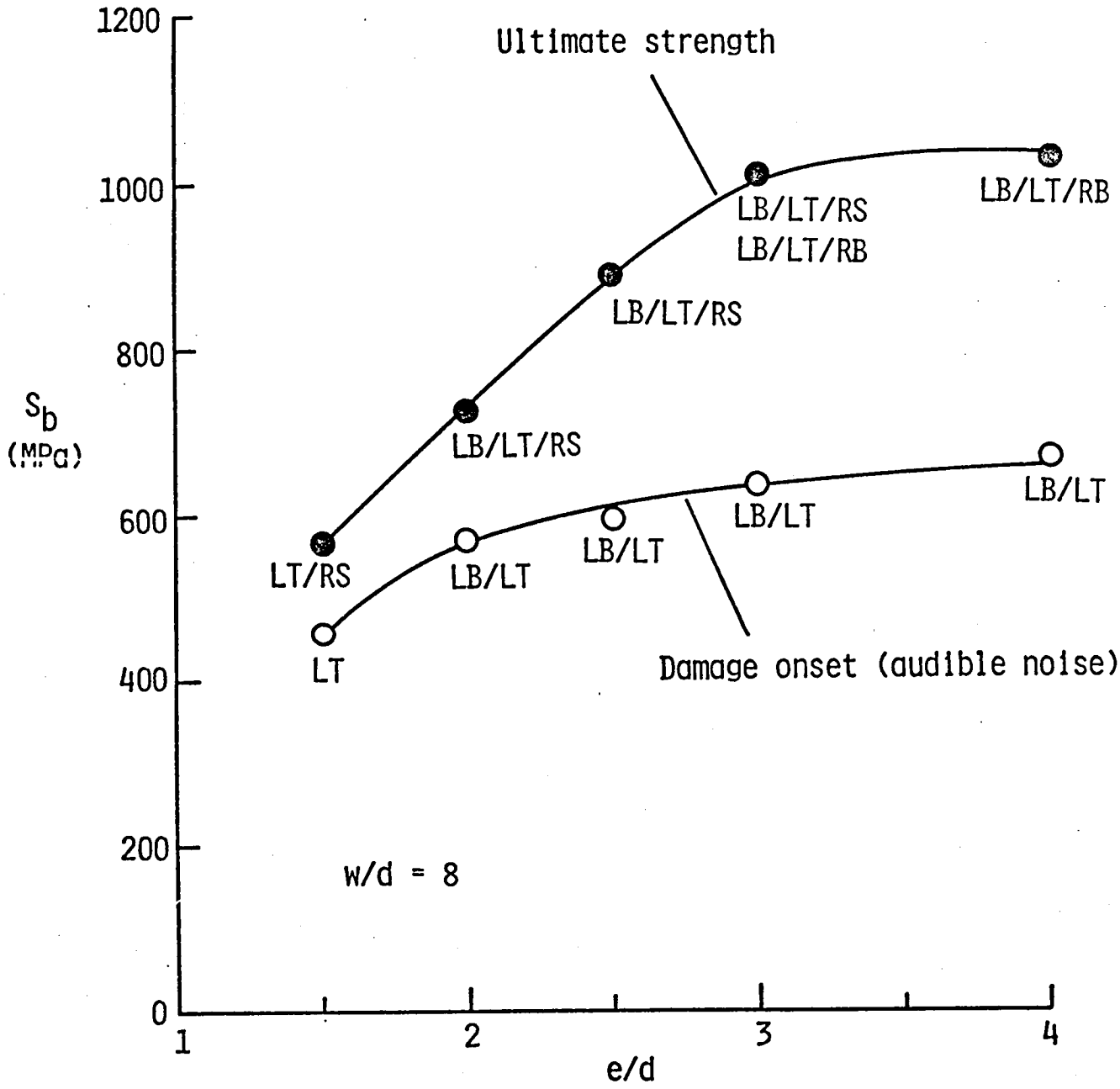

Figure 10. - Damage onset and ultimate strength for a range of e/d values.

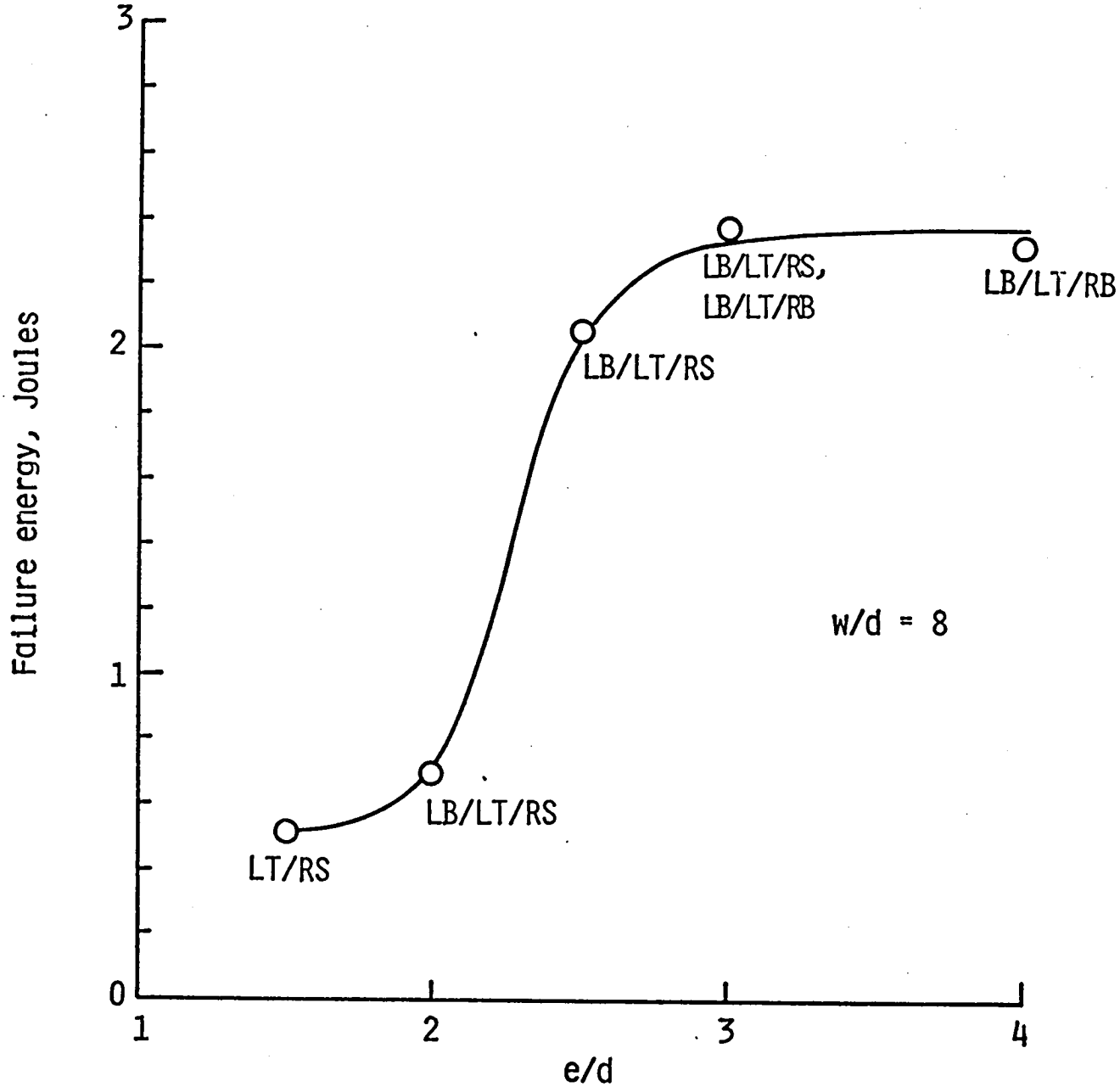

Figure 11. - Failure energy for range of e/d values.

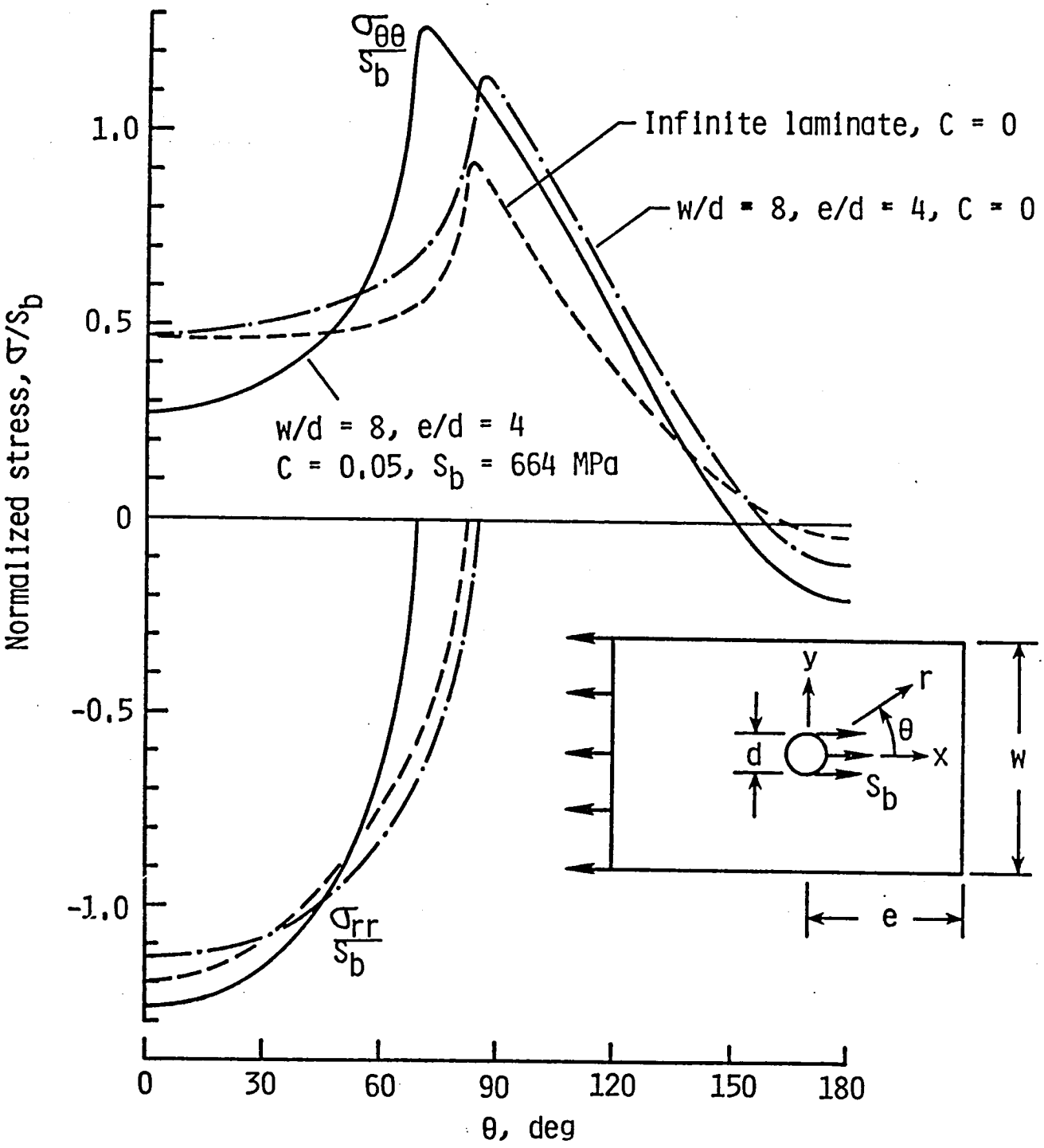

Figure 12. - Stress distributions along hole boundary.

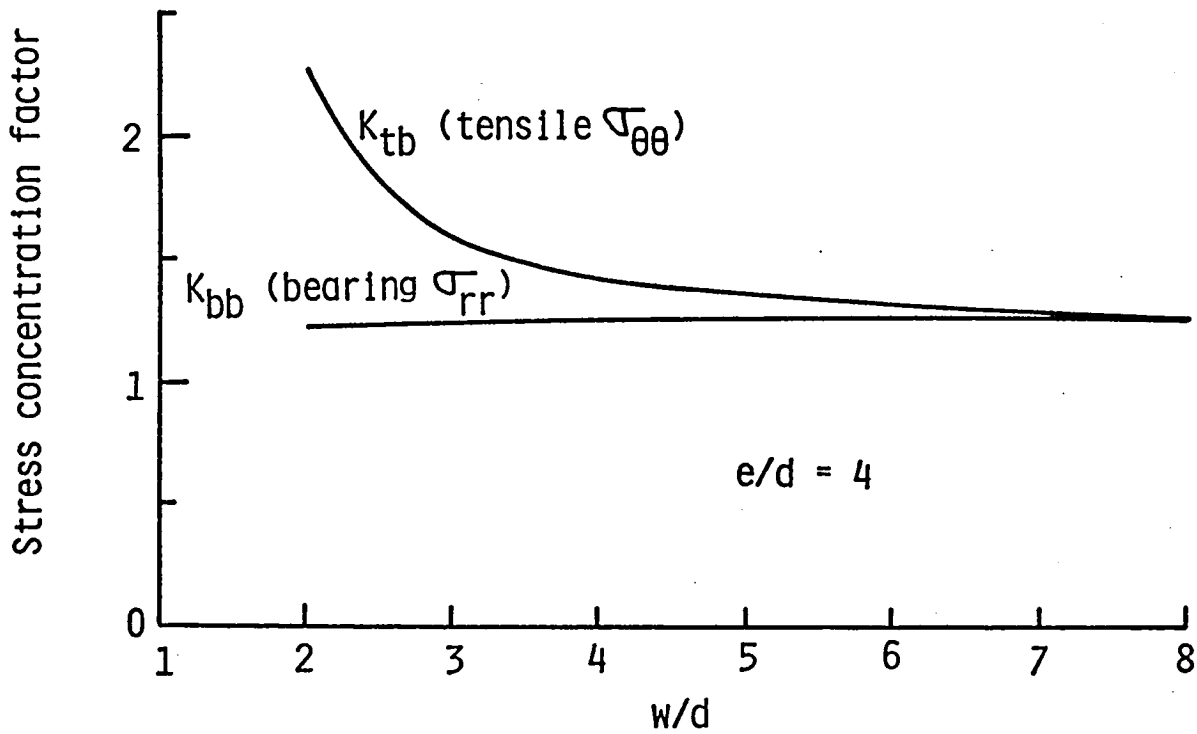

(a) Results for w/d range.

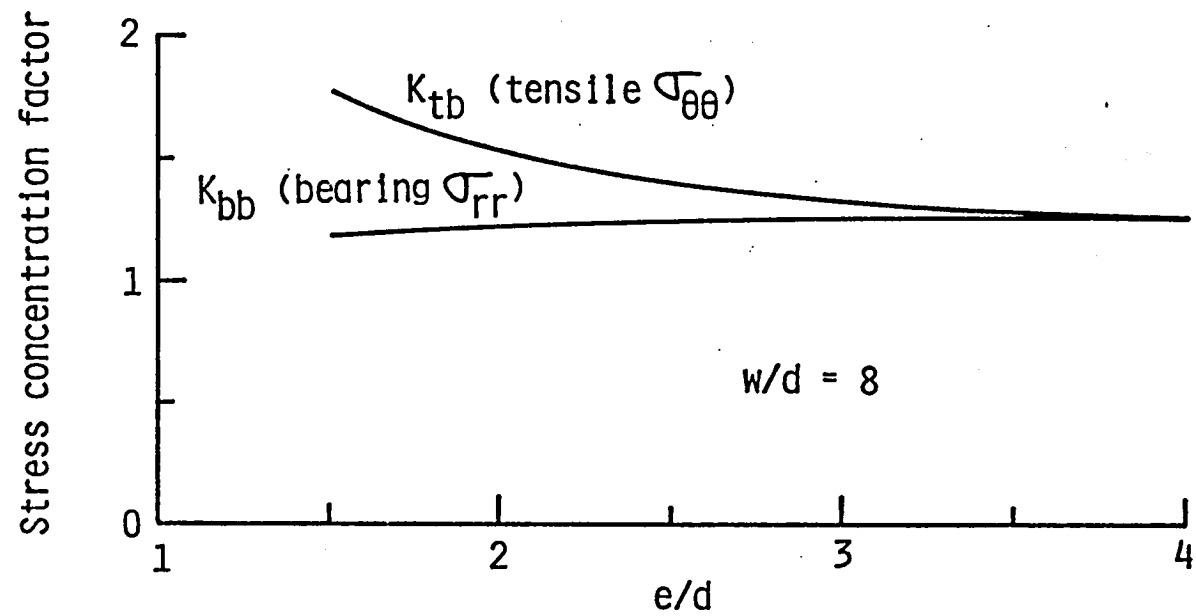

(b) Results for e/d range.

Figure 13. - Stress concentration factors for test specimens.

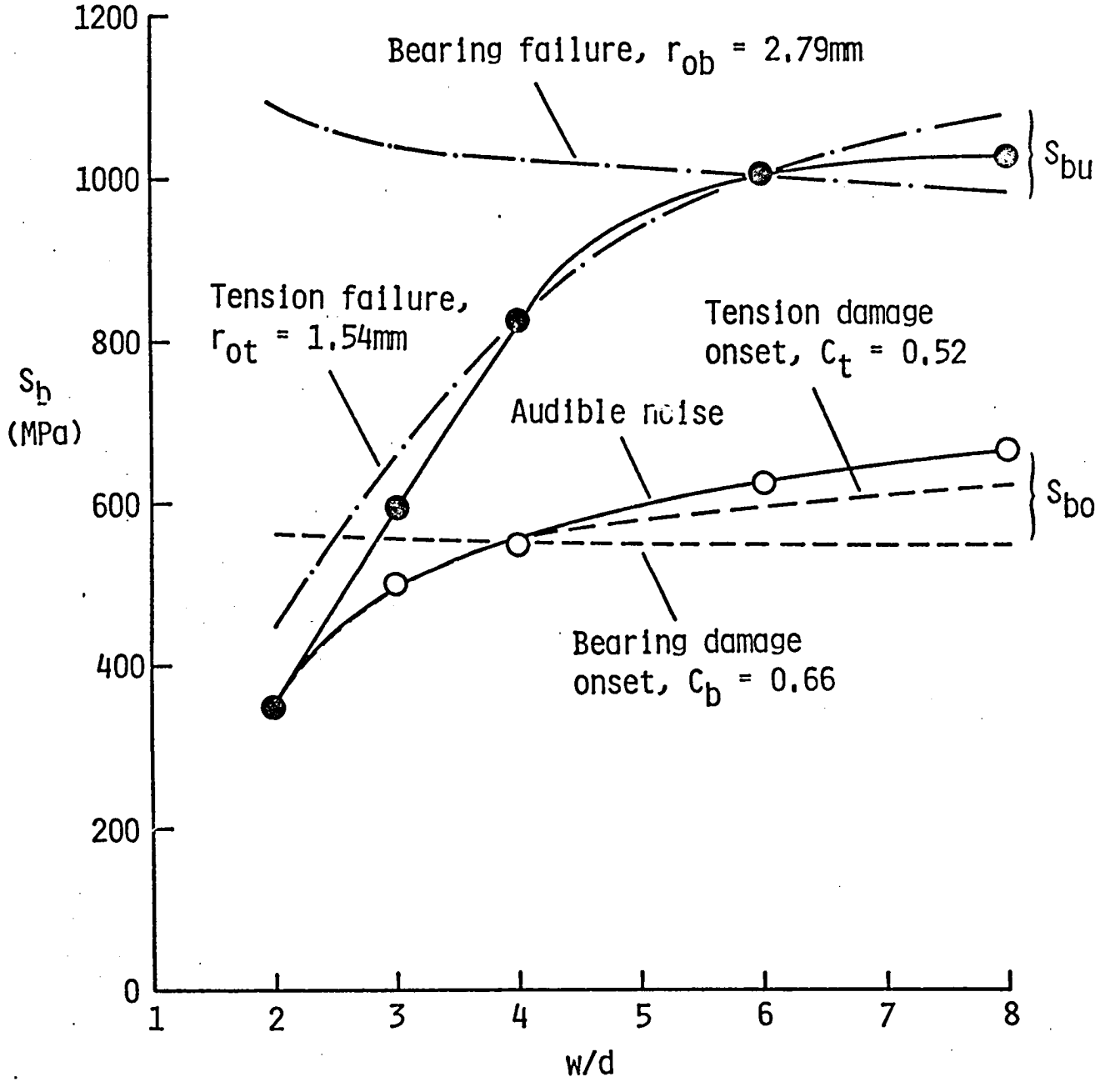

Figure 14. - Strength predictions for w/d range.

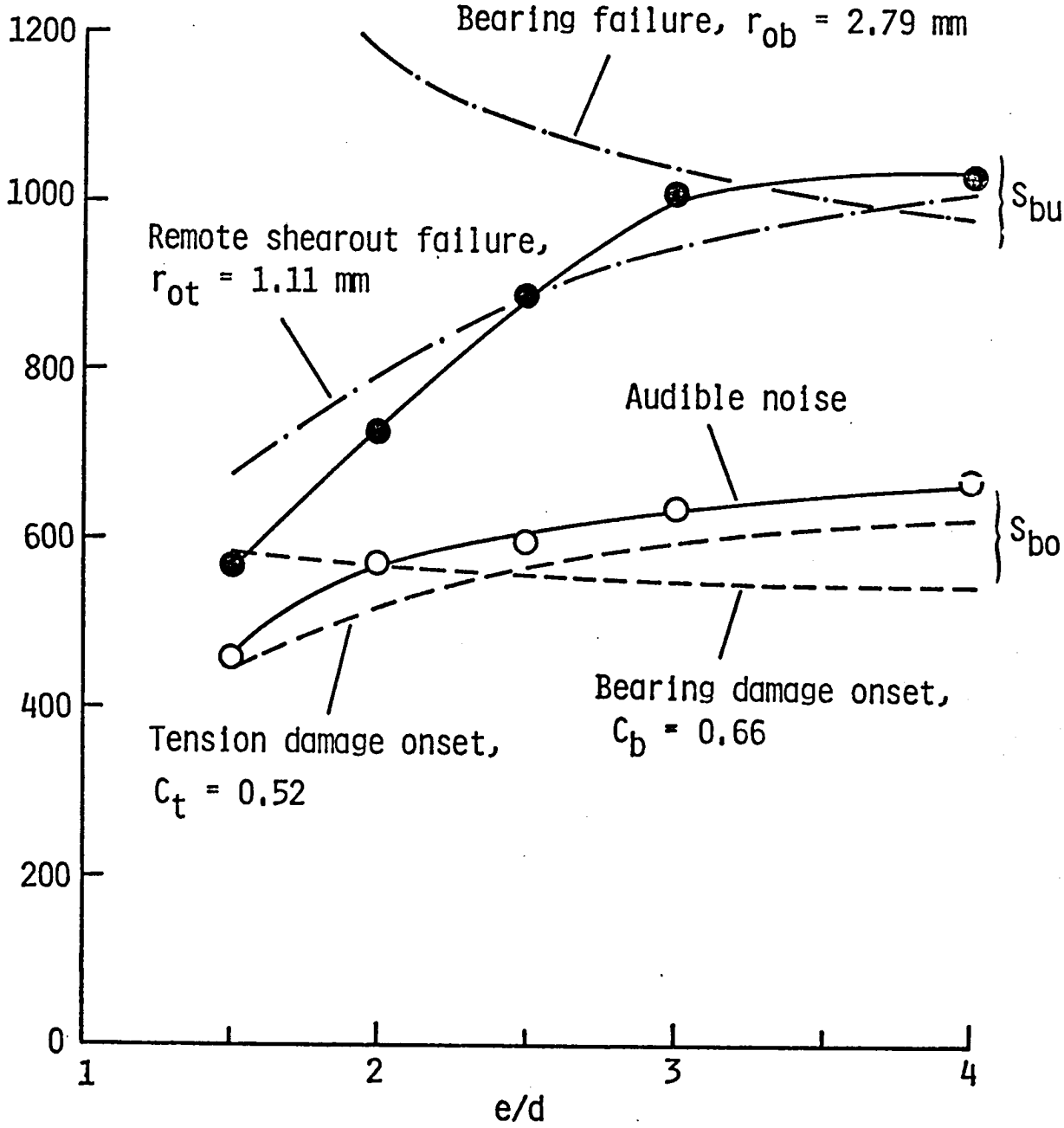

Figure 15. - Strength predictions for e/d range.

1. Report No.	2. Government Accession No.	3. Recipient's Catalog No.
NASA TM-86297		

4. Title and Subtitle	5. Report Date
Failure Analysis of a Graphite/Epoxy Laminate Subjected to Bolt Bearing Loads	August 1984
	6. Performing Organization Code: 505-33-33-05

7. Author(s)	8. Performing Organization Report No.
J. H. Crews, Jr. R. V. A. Naik*	

9. Performing Organization Name and Address	10. Work Unit No.
NASA Langley Research Center Hampton, VA 23665	
	11. Contract or Grant No.
	13. Type of Report and Period Covered: Technical Memorandum
12. Sponsoring Agency Name and Address	14. Sponsoring Agency Code
National Aeronautics and Space Administration Washington, DC 20546	

15. Supplementary Notes

*R. V. A. Naik, Graduate Student, Old Dominion University, Norfolk, VA

16. Abstract

Quasi-isotropic graphite/epoxy laminates (T300/5208) were tested under bolt-bearing loads to study failure modes, strengths, and failure energy. Specimens had a range of configurations to produce failures by the three nominal failure modes: tension, shearout, and bearing. Radiographs were made after damage onset and after ultimate load to examine the failure modes. Also, the laminate stresses near the bolt hole calculated for each test specimen configuration, and then used with a failure criteton analyze the test data.

Failures involving extensive bearing damage were found to dissipate significantly more energy than tension dominated failures. The specimen configuration influenced the failure modes and therefore also influenced the failure energy. In the width-to-diameter ratio range of 4 to 6, which is typical of structural joints, a transition from the tension mode to the bearing mode was shown to cause a large increase in failure energy.

The failure modes associated with ultimate strength were usually different from those associated with the damage onset. Typical damage sequences involved bearing damage onset at the hole boundary followed by tension damage progressing from the hole boundary. Ultimate failures involved shearout beyond the clampup washer for specimens with small edge distances and involved bearing damage beyond the washer for larger specimens. Strength predictions indicated that the damage corresponding to ultimate strength was governed by the maximum stress near the hole.

17. Key Words (Suggested by Author(s))	18. Distribution Statement
laminate, bolt, bearing, graphite/epoxy, strength, damage, stress analysis, composites	Unclassified - Unlimited Subject Category 24

19. Security Classif. (of this report)	20. Security Classif. (of this page)	21. No. of Pages	22. Price
Unclassified	Unclassified	34	A03

For sale by the National Technical Information Service, Springfield, Virginia 22161